Electrocatalysis (2016) 7:287–296
DOI 10.1007/s12678-016-0304-3

ORIGINAL RESEARCH

The Effect of Platinum Loading and Surface Morphology on Oxygen Reduction Activity

S. Taylor[1] · E. Fabbri[2] · P. Levecque[1] · T. J. Schmidt[2,3] · O. Conrad[1]

Published online: 16 March 2016

Abstract The catalytic activity of Pt catalysts towards the oxygen reduction reaction (ORR) was investigated on a catalyst system developed by thermally induced chemical deposition of Pt on carbon. The use of this deposition method made it possible to prepare a practical catalyst system with various Pt loadings on the support. Increasing the Pt loading caused a change in the Pt surface morphology which was confirmed by transmission electron microscopy (TEM) and CO stripping voltammetry measurements. The occurrence of a low and high-potential CO oxidation peak suggested the presence of Pt agglomerates and Pt nanoparticles, respectively. An increase in Pt loading lead to a subsequent decrease in the electrochemical surface area (ECSA, m^2_{Pt}/g_{Pt}) as the platinum surface transitioned from isolated platinum nanoparticles to platinum agglomerates. The specific activity was found to increase with increasing Pt loadings, while the mass activity decreased with loading. The mass and specific activity data from this study was found to follow a 'master curve' obtained by the comparison of normalised activities from various different studies in the literature. Pt selectivity was also affected by Pt loading and hence Pt surface morphology. At low Pt loadings, i.e. large interparticle distances, the amount of H_2O_2 produced was significantly higher than for high Pt loadings. This confirms the presence of a 'series reaction pathway' and highlights the importance of the H_2O_2 desorption-readsorption mechanism on Pt nanoparticles and the ultimate role of Pt interparticle distance on the ORR mechanism.

Keywords Platinum · Oxygen reduction reaction · Hydrogen peroxide · Thermally induced chemical deposition

Introduction

To date, the cost of the high platinum loadings in polymer electrolyte fuel cells (PEFCs) remains one of the main hurdles to their broad commercialisation. The oxygen reduction reaction (ORR) occurring on the cathode side of a fuel cell (Eq. 1) is one of the most extensively researched electrochemical reactions owing to its significance in fuel cell operation [1, 2].

$$\tfrac{1}{2}\,O_2 + 2\,H^+ + 2\,e^- \rightarrow H_2O \quad (1)$$

Platinum is the most commonly used electrocatalyst for the ORR, owing to its high activity towards the ORR and high stability under cathode operating conditions. Much attention has been paid to this reaction as a result of high reaction overpotentials (0.3–0.4 V) caused by the sluggish kinetics of the ORR, which inherently leads to the need for high catalysts loadings of 0.1–0.5 mg/cm^2 on the cathode side of the fuel cell in order to attain reasonable performance levels (0.2 g/kW) [3]. This increases the cost of production of PEFCs, ultimately

Electronic supplementary material The online version of this article (doi:10.1007/s12678-016-0304-3) contains supplementary material, which is available to authorized users.

✉ P. Levecque
pieter.levecque@uct.ac.za

[1] HySA/Catalysis Centre of Competence, Centre for Catalysis Research, Department of Chemical Engineering, University of Cape Town, 7701 Rondebosch, Cape Town, South Africa

[2] Electrochemistry Laboratory, Paul Scherrer Institute, 5232 Villigen, Switzerland

[3] Laboratory of Physical Chemistry, ETH Zürich, 8093 Zürich, Switzerland

hindering their large-scale commercialization [4]. Platinum particle size and surface morphology are thought to be directly related to the catalytic activity of platinum towards the ORR [5]. A better understanding of the effects of platinum particle size and surface morphology on the mechanism and kinetics of the ORR is critical if platinum loadings are to be reduced at the cathode, while maintaining the US Department of Energy (DoE) target performance levels [6]. Over the past few decades, several research groups have contributed to a better understanding of the electrochemical behaviour of platinum catalysts with respect to the ORR [3–7].

It has been widely reported by many authors that there still exists a discrepancy between the effects of particle size on the ORR activity of platinum catalysts [4, 8–13]. According to an early review study by Kinoshita [10], it was assumed that platinum particles were cubo-octahedral in shape, and changes in crystallite size lead to a consequent change in the respective ratios of Pt(111) and Pt(110) surface facets and this was thought to be directly related to mass (A/gPt) and specific activity ($\mu A/cm^2Pt$) of highly dispersed platinum catalysts. A maximum mass activity was observed for particles of approximately 3.5 nm in several studies and was attributed to the maximum surface atoms present for the Pt(111) and Pt(110) crystal faces [10–12]. In a more recent study by Shao et al. [13], using density functional theory (DFT) calculations on a cubo-octahedral nanoparticle, a maximum in mass activity was determined at a particle size of 2.2 nm. However, in a study by Schwanitz et al. [14], a maximum in mass activity was not observed at any particle size, instead a decrease in mass activity with particle size was seen. It should be noted that the experimental conditions and preparation methods in all studies differ, which is a major factor that could affect the inconsistencies in the results observed for the particle size effect in different studies. Nonetheless, it is evident that the effects of particle size on ORR activity remain unclear.

There have been fewer investigations into the effects of interparticle distance of platinum nanoparticles on the ORR activity and selectivity [4, 5, 15]. Nesselberger et al. [5] reported that when using well defined, size-selected platinum nanoclusters, the ORR activity is influenced by the interparticle distance, with closely packed platinum nanoclusters showing high mass activities resembling that of bulk platinum. It was suggested that the distribution of the electrochemical potential in the electrochemical double layer located between the nanoclusters can influence the coverage of the electrode by oxygenated species, consequently affecting activity [5]. Yang et al. [4] investigated the interparticle distance effect on hydrogen peroxide formation and found that the extent of hydrogen peroxide formation increased with decreased particle size and increased interparticle distance. This observation was attributed to the interparticle distance-dependent mass transport of H_2O_2 species. Hydrogen peroxide formation during the ORR is known to adversely affect the ORR activity to water (Eq. 2). H_2O_2 species form via a two-electron process, thus reducing overall ORR efficiency.

$$O_2 + 2\,H^+ + 2\,e^- \leftrightarrow H_2O_2 \tag{2}$$

It is thought that particle size and interparticle distance play a significant role in the formation of hydrogen peroxide species [8, 13, 15]. It is however unclear which effect dominates. In a recent study, it was reported that a decrease in Pt loading lead to a higher coverage of anionic impurities which inhibit H_2O_2 reduction and enhance the desorption of H_2O_2 intermediates at potentials higher than those typical of the H_{upd} region [16]. Rotating ring disk electrode (RRDE) measurements can be used to quantify H_2O_2 formation during the ORR. Inaba et al. [15] proposed that H_2O_2 formation increases as particle agglomeration decreases. This can be explained in terms of the proximity of adjacent platinum particles. If a H_2O_2 species forms and does not come into contact with a neighbouring platinum active site, the H_2O_2 molecule will diffuse into the bulk solution without being further reduced to H_2O. Another stance is that the oxophilicity of platinum particles is highest for small particle sizes [8]. In a study by Shao et al. [13], the oxygen-binding energy of Pt-O for all surface sites was seen to decrease with particle size. Thus, for small platinum particles (<3 nm), platinum active sites have a higher probability of being blocked by oxygenated species, thus preventing any O_2 reactant or H_2O_2 species formed during the ORR being adsorbed and further reduced to H_2O. The ORR mechanism itself is still unclear, and in order to reduce H_2O_2 production, it is prudent that a better understanding of the factors affecting hydrogen peroxide formation is thoroughly investigated.

CO stripping voltammetry measurements have been suggested as a useful indication of the extent of particle agglomeration for supported platinum catalysts [16]. Multiple CO oxidation peaks have been observed by a number of authors [17–19], for supported platinum on carbon catalysts. Maillard et al. [17] found that CO stripping on platinum agglomerates alone produced a single low-potential CO oxidation peak at 0.76 V vs. RHE. This suggested that CO oxidation occurs more easily on platinum agglomerates compared to isolated platinum particles, which showed a CO oxidation peak at 0.86 V vs. RHE. Platinum agglomerates contain a greater number of step and edge sites which enhance OH adsorption [13], which is in turn thought to facilitate the CO oxidation reaction shown below by Eqs. 3 and 4, where the * indicates an active site for the reaction [18].

$$H_2O + * \leftrightarrow OH_{ads} + H^+ + e^- \tag{3}$$

$$CO_{ads} + OH_{ads} \rightarrow CO_2 + H^+ + e^- + 2* \tag{4}$$

However, Urchaga et al. [20] suggest that it is in fact the different crystal sites present on the different platinum

surfaces that affect the CO oxidation potential. According to Urchaga et al. the Pt(111) sites were found to be responsible for the low potential peak and the low-coordination sites were accountable for the high-potential CO oxidation peak [20]. Nonetheless, the peak multiplicity appears to be an indication of the extent of particle agglomeration and particle size effects in both studies.

Following the current literature, it is prudent that further investigations with regard to the effect of different platinum surfaces on the ORR activity and selectivity be carried out. It is also important to establish CO stripping voltammetry as a quantifiable, electrochemical method for determining the relative amount of the different platinum surfaces present in a supported catalyst system, in order to fully understand the effects of such platinum surfaces on the ORR activity.

In a recent publication by our groups, the effect of increased platinum loading and agglomeration on the ORR and hydrogen peroxide formation was investigated for a sputtered model electrode system [21]. A decrease in the electrochemical active surface area was seen as the surface transitioned from dispersed platinum nanoparticles to an extended platinum surface. Hydrogen peroxide formation was seen to be greatest on the low loading, isolated platinum nanoparticle surface. Findings from this study support the presence of a serial reaction pathway for the ORR via a H_2O_2 intermediate on a peroxide desorption-readsorption pathway [21]. Extending this study to a practical catalyst system, we here present a study based on the preparation of platinum supported on carbon catalysts by thermally induced chemical deposition with increasing platinum loadings on the support. CO stripping voltammetry was used to look at the extent of particle agglomeration by studying the different CO oxidation peak potentials. RRDE measurements were employed to evaluate the hydrogen peroxide formation on the different platinum surfaces and shed light on the mechanism of the ORR.

Experimental

Full experimental procedures for catalyst preparation and physical characterisation as well as more details on the electrochemical analysis are described in the Electronic Supplementary Information.

Electrochemical Characterisation

All experiments were performed in a standard three-electrode setup at room temperature in a 0.1 M $HClO_4$ solution. Pt gauze was used as the counter electrode. A mercury/mercurous sulphate reference electrode was used, and all potential values were reported against the reversible hydrogen electrode, RHE. A Biologic SP300 bipotentiostat was coupled to a Pine Instruments MSR rotator. A Pine Instruments RRDE tip (E7R9, d_{GC} = 5.61 mm, Pt ring) was used as working electrode (WE). Before use, the WE was polished to a mirror finish. The catalyst ink was prepared for each catalyst sample using the same recipe following an adapted method for preparation of thin-film RDEs [22]: 10-mg catalyst powder was weighed in a glass vial; 10 mL of 18.2 MΩ.cm water, 3 mL isopropanol and 50 μL Nafion® (Dupont) solution were added to the weighed catalyst powder and the mixture was ultra-sonicated for 20 min. Ten microlitre of catalyst ink was pipetted onto the mirror-polished GC disk, and the electrode was then dried in air while being rotated at 700 rpm [23]. Pt loadings in the prepared thin film RDEs were calculated to be 7.8, 15.6 , 23.5 and 31.3 μg/cm^2 for the respective catalyst samples 20, 40, 60 and 80 wt% Pt samples.

Cyclic Voltammetry

The potential of the working electrode (WE) was cycled between 0.05 and 1.0 V vs. RHE at 100 mV/s to electrochemically clean the catalyst surface of any surface impurities. The sweep rate was then reduced to 50 mV/s, and the third cycle at that scan rate was used for analysis. The electrochemically active surface area (ECSA) was calculated by integrating the CV in the hydrogen underpotential deposition (H_{upd}) region, assuming a monolayer hydrogen charge of 210 μC/cm$^2_{Pt}$ [24].

CO Stripping Voltammetry

CO gas at ambient pressure was bubbled into the electrolyte solution for 20 min for all loadings while holding the potential of the working electrode at 0.1 V vs. RHE. The electrolyte was then purged with argon gas for 20 min while maintaining the potential of the WE at 0.1 V vs. RHE. The peak area was calculated using a baseline CV recorded in argon at the same scan rate, 20 mV/s, and a normalisation factor of 420 μC/cm$^2_{Pt}$ was used to calculate the ECSA. Although widely used, the normalisation factor might have a certain degree of error related to it; however, in this study, the results are only used to compare prepared catalysts relative to each other.

Linear Sweep Voltammetry

The WE was immersed in the electrolyte under potential control (0.5 V vs. RHE). ORR curves were measured at rotation speeds of 400, 900, 1600 and 2500 rpm. The potential of the WE was swept from 1.0 to 0 V vs. RHE and back at 5 mV/s. The cathodic sweep was used to analyse the mass and specific activities of the Pt/C catalysts. The ORR curves obtained in an oxygen-saturated electrolyte were corrected for the capacitive current associated with Pt/C catalysts, by subtracting a CV measured in an argon-saturated electrolyte. All curves were ohmic drop corrected.

Rotating Disk and Ring Disk Electrode Measurements

The WE was immersed in the electrolyte under potential control (0.5 V vs. RHE) in an oxygen-saturated electrolyte solution. The ring was held at a potential of 1.2 V vs. RHE throughout the measurements, while the disk potential was swept from 1.0 to 0 V vs. RHE at 5 mV/s. The disk and ring currents were recorded as a function of the disk potential. The collection efficiency was measured as in the work by Paulus et al. [25] and was found to be 0.37 ± 0.02 for this system. All RRDE experiments were carried out at one rotation speed (1600 rpm) and gave identical results to the RDE curves at the same rotation speed [26].

Results and Discussion

Overview

Table 1 below gives an overview of the data obtained for the different prepared catalysts. Specific trends in the data are discussed in detail in the following sections. The sections below will first outline the physical characterisation and serve as a means to explain some of the results obtained in the electrochemical characterisation section.

Physical Characterisation

The TGA results confirmed that the required platinum loading was deposited on the carbon surface with an error of approximately ±1 % in all cases. The TEM images in Fig. 1 illustrate the progression from the 20 to the 80 Pt wt% prepared catalysts. Figure 2 shows the particle size distribution obtained for all samples. All catalysts show a normal distribution, and a primary Pt particle size observed was between 3.4 and 3.9 nm. The same trend is seen in the XRD results (Table 1). The deviation between XRD and TEM results, especially at higher loadings, is due to difficulties in identifying Pt particles in the clusters visible on the TEM images. It is evident from Figs. 1 and 2 that as the platinum loading increases from 20 to 80 wt% Pt, the particles are becoming more agglomerated. It is furthermore clear from TEM that regardless of the agglomeration, there is a clear increase in Pt coverage on the carbon support.

The TEM images were also used to measure the average interparticle distance obtained at the different loadings. Interparticle distance was measured as open space between particles. The results are shown in Table 2. In correspondence to the TEM images, it is clear that at the lower loadings, the particles are much more distributed across the support surface and spaced further away from each other.

Electrochemically Active Surface

Cyclic voltammograms were recorded for each of the prepared catalysts and the results are shown in Fig. 3.

The profile of the voltammograms confirms the presence of polycrystalline Pt for all samples. The ECSA (m^2_{Pt}/g_{Pt}) is seen to decrease with an increase in Pt loading, this can be explained by the increase in particle agglomeration with loading, confirmed by TEM images in Fig. 1, and hence an overall reduction in the active Pt surface area. This effect was also observed by our groups in a study on sputtered model electrodes with increasing Pt loadings [21]. López-Cudero et al. also reported on a system with increasing Pt loading on carbon (from 10 to 50 wt%) but did not observe the trend of decreasing ECSA with higher loading [27]. The authors observed similar particle sizes for all catalysts prepared (10–50 wt%). This indicated that even when agglomerated, the particles maintain the behaviour of a single particle. This was further shown by cyclic voltammetry where no changes in the voltammetric profile where observed, nor did any preferential domains occur. We attribute this different finding to the preparation method used in our work as compared to the one by López-Cudero et al. We applied a one-step simultaneous reduction-deposition process while López-Cudero et al. used a stabiliser to prepare particles which were consequently deposited. Especially at the level of the agglomerated catalyst, the difference in preparation method clearly leads to a different morphology.

From the cyclic voltammograms, the Pt-oxide peak occurs at a lower potential for the low loading catalysts (20 and 40 wt% Pt) compared to the high loading catalysts (60 and 80 wt% Pt). This effect is not as pronounced as in our previous

Table 1 Summary of characterisation results

wt%	Particle size (XRD, nm)	Particle size (TEM, nm)	ECSA (H_{upd}, m^2/g)	ECSA (CO, m^2/g)	$i_{k,spec}$ ($\mu A/cm^2_{Pt}$)	$i_{k,mass}$ (mA/mg_{Pt})
20	3.4	3.4	62	82	16.1	9.99
40	4.1	3.6	55	70	17.0	9.33
60	4.6	3.7	40	43	20.5	8.18
80	5.4	3.9	31	30	26.3	8.15

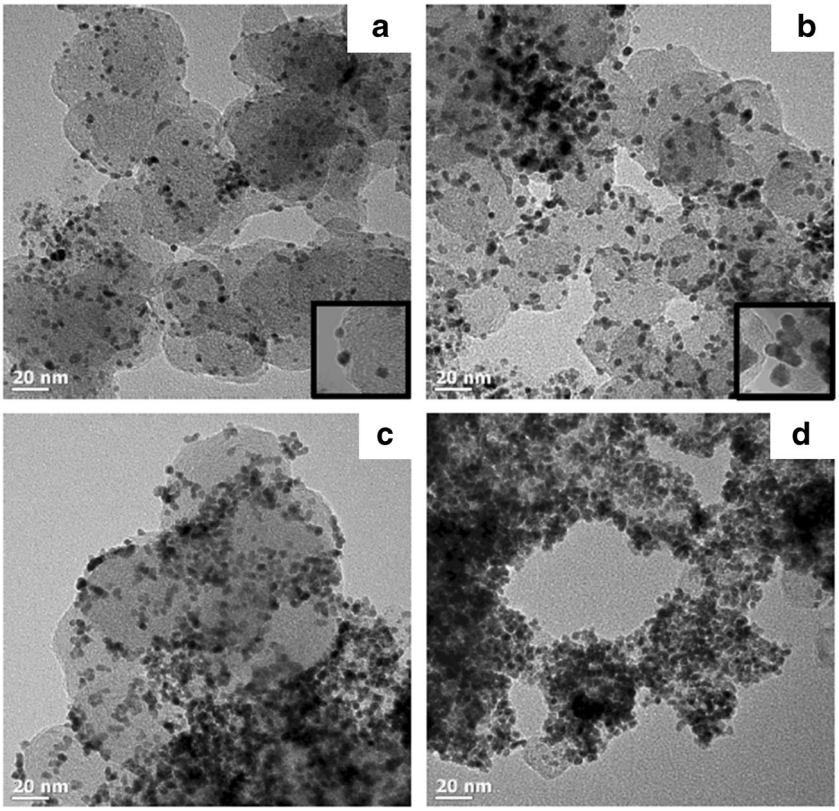

Fig. 1 TEM images of **a** 20, **b** 40, **c** 60 and **d** 80 wt% Pt catalysts, respectively

study [21]; however, the same conclusions could be drawn to explain the shift in the Pt-oxide peak. Isolated nanoparticles have a higher adsorption energy for oxygenated species compared to Pt agglomerates and extended surfaces; hence, the Pt-O peaks will occur at lower potentials for samples containing Pt nanoparticles [8, 13, 21, 28].

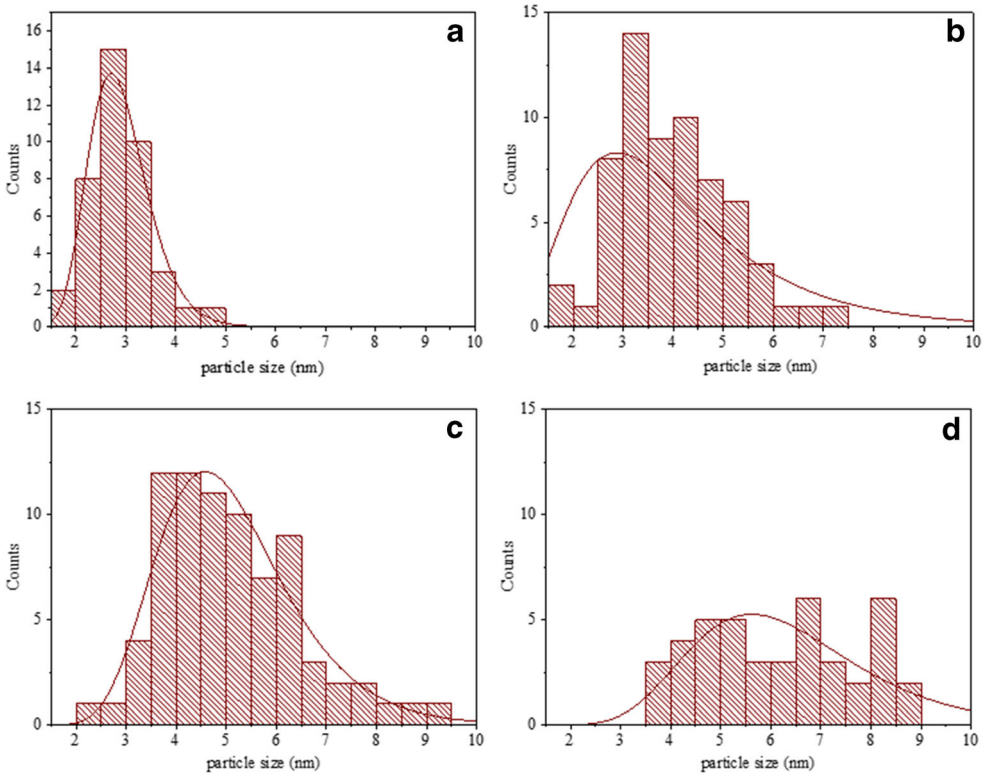

Fig. 2 Particle size (diameter) distribution based on TEM images of **a** 20, **b** 40, **c** 60 and **d** 80 wt% Pt catalysts, respectively

Table 2 Interparticle distances measured by TEM

wt%	Average interparticle distance (nm)	St dev (nm)
20	9.7	4.3
40	8.6	3.2
60	6.0	1.9
80	4.0	1.1

It has been shown that CO stripping could be used to investigate the change of morphology of a Pt surface, i.e. detect the presence of particle agglomerates or isolated nanoparticles [17, 20, 21]. Therefore the catalysts prepared for this work were also characterised using CO stripping voltammetry to investigate and compare the trends with the model catalyst system developed previously by our groups [21]. The results are shown in Fig. 4 below.

Figure 4a illustrates the CO stripping voltammograms for a full sweep from 0 to 1.0 V. Figure 4b focuses on the CO oxidation peaks occurring between 0.6 and 0.86 V. Multiple CO oxidation peaks are observed in Fig. 4 between 0.6 and 0.86 V. It is noted that the low potential peak, peak I, increases in intensity as the platinum loading increases from 20 to 80 wt% Pt. Peak multiplicity in CO stripping experiments has been a topic of debate in the literature [17–21]. According to Maillard et al. [17], it is the platinum agglomerates which cause the low-potential CO oxidation peak. Similarly to the cyclic voltammograms above, our results differ from those obtained by López-Cudero et al. [27] due to the different preparation process.

The TEM images (vide supra) indicate an increase in particle agglomeration with increasing Pt loading which supports the theory behind the occurrence of the low-potential CO oxidation peak for higher platinum loadings. Furthermore,

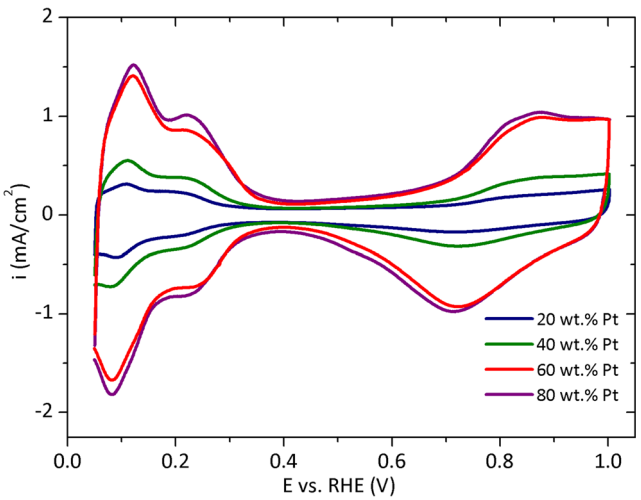

Fig. 3 Cyclic voltammograms carried out in an Ar-saturated 0.1 M $HClO_4$ solution at room temperature, sweep rate 50 mV/s for different wt% Pt catalysts. Comparison of CV's for 20, 40, 60 and 80 wt% Pt

Urchaga et al. [20] reported that the multiple peaks could be related to different crystal facets present at the platinum surface, with the low potential peak being related to Pt(111) sites. Studies on the relationship between particle size and preferred particle shape have indicated that more of the Pt(111) faces are exposed on the surface of larger Pt particles than for small Pt nanoparticles [10]. It is also known that the Pt(111) face is more thermodynamically stable and therefore would be the favoured exposed surface if particles were to agglomerate [29]. It is likely that the low-potential CO oxidation peak (i.e. weakly adsorbed CO) observed is in fact due to the presence of platinum agglomerates which in turn contain a greater amount of Pt(111) faces compared to isolated platinum nanoparticles, thus relating the two theories proposed by Maillard et al. [17] and Urchaga et al. [20]. The low potential peak also suggests that CO oxidation is significantly enhanced on the surface of Pt agglomerates compared to isolated Pt nanoparticles. As the results obtained are in line with both Maillard et al. [17] and Urchaga et al. [20], we have shown that CO stripping can be used as a fingerprint for the extent of particle agglomeration, as we have shown previously [21]. This is an additional tool which validates the presence of the different Pt surfaces on an electrochemical level rather than just a physical, visual level (TEM).

Electrocatalytic Activity Trends

Figure 5 shows the cathodic sweeps of the ORR polarisation curves recorded at a rotation speed of 1600 rpm.

For all samples, a typical profile showing kinetic control at low overpotentials and a mass transport control at high overpotentials can be seen. It is clear that the lower loading catalysts (20 wt% and 40 wt%) do not reach the theoretical limiting current of 6.02 mA/cm^2. According to the Levich equation, diffusion-limited current is by definition not a function of platinum loading. However, limiting current can be influenced by Pt particle distribution and coverage, and hence, in the case of isolated Pt nanoparticles, the geometric surface area is overestimated. Furthermore, mass transport limitations because of Nafion in the catalyst thin film can also be excluded as the Nafion added was merely as a binder [25]. The lower Pt loading catalyst do not reach limiting currents; we will later (RRDE experiments) show that the main contributor to this is the high prevalence of the two-electron pathway towards hydrogen peroxide formation at these loadings. The findings for the practical system discussed here are in line with the observations made in a model system our groups previously reported on [21]. The kinetic current density i_k could be obtained using the Koutecky-Levich equation (Eq. 5) to correct the experimentally obtained current density for mass transport influences.

$$\frac{1}{i} = \frac{1}{i_k} + \frac{1}{i_d} \tag{5}$$

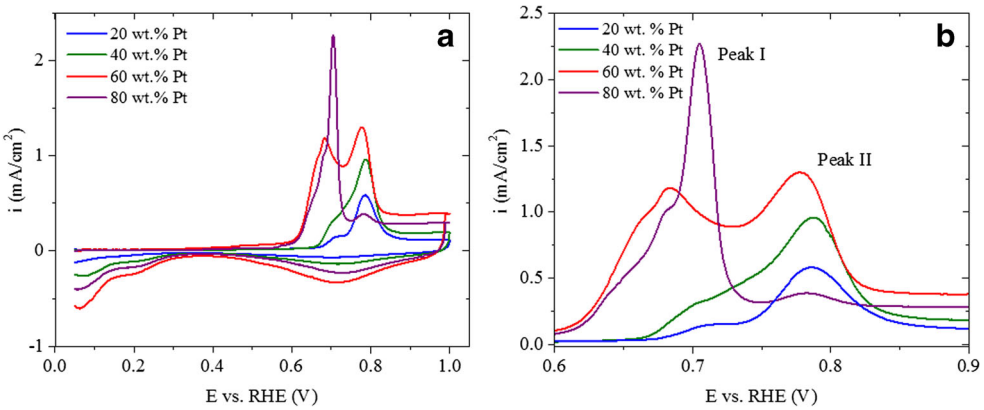

Fig. 4 **a** CO stripping voltammograms in an Ar-saturated 0.1 M $HClO_4$ solution at a sweep rate of 20 mV/s for 20, 40, 60 and 80 wt% Pt catalysts, at room temperature. **b** CO oxidation peaks 20, 40, 60 and 80 wt% Pt catalysts, where *Peak I* indicates the low potential peak and *Peak II* indicates the high potential peak

The result is plotted in Fig. 5b and comparing i_k at 0.9 V shows increasing i_k with increasing Pt loading, i.e. an increase in i_k from isolated nanoparticles to Pt agglomerates.

In Fig. 6, the surface-specific current density $i_{k,spec}$, and the mass-specific current density, $i_{k,mass}$, are plotted as a function of the ECSA. For comparison, the trends from our study on the sputtered model system [21] have been added as inserts.

Assuming identical reaction kinetics and surface properties of the different Pt loading catalysts, one would expect the $i_{k,spec}$ to remain constant, independent of Pt loading. However, Fig. 6a indicates that the surface-specific activity decreases with higher ECSA (decreasing Pt loading). In other words, the more dispersed the Pt nanoparticles, the lower the specific activity of the catalyst. The 80 and 60 wt% Pt catalysts show similar surface activities indicating similar surface properties of the two catalysts. These results are in line with previous studies which include our own study on model substrates [5, 14, 21] that reported an increase in specific activity with increased Pt loading.

Figure 6b shows the mass-specific activity as a function of the loading, with the lower ECSA related to the higher Pt loading. From Fig. 6b, it can be seen that there is a clear distinction between the low ECSA catalysts (60 and 80 wt% Pt loading) and the higher ECSA catalysts (20 and 40 wt% Pt loading). The mass activity for the former is clearly lower. The larger particle size (XRD and TEM), increased agglomeration (TEM) and lower interparticle distance for the catalysts with higher wt% Pt lead to a relatively lower amount of the Pt accessible for reaction for the higher loading catalysts as compared to the lower loadings, which have predominantly dispersed nanoparticles. Therefore, a significant amount of Pt does not take part in the ORR, and hence, a lower mass activity is observed for the high loading catalysts.

A comparison of the results from this study with a previous study by our groups concerning the morphological effects of sputtered model electrodes on the ORR activity [21] reveals that lower mass and specific activities are observed in this study compared to the previous study. A possible explanation is that the lower activities might be caused by the interparticle distance effect. For comparable ECSA values, the catalytic system presented here would inherently have platinum particles at larger distances from one another relative to the sputtered model electrode system. In the latter, Pt particles have been deposited onto a preformed layer of Vulcan XC72

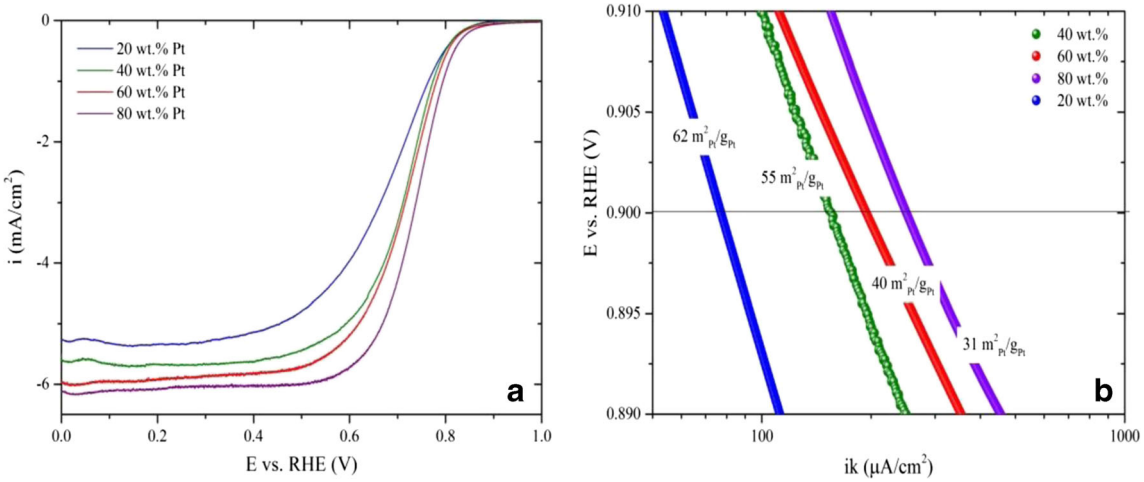

Fig. 5 **a** Cathodic sweep ORR curves for different Pt loadings (scan rate 20 mV/s, RT, 1600 rpm, O_2-saturated 0.1 M $HClO_4$). **b** Tafel Plots of mass diffusion and ohmic drop corrected kinetic current (i_k) vs. potential

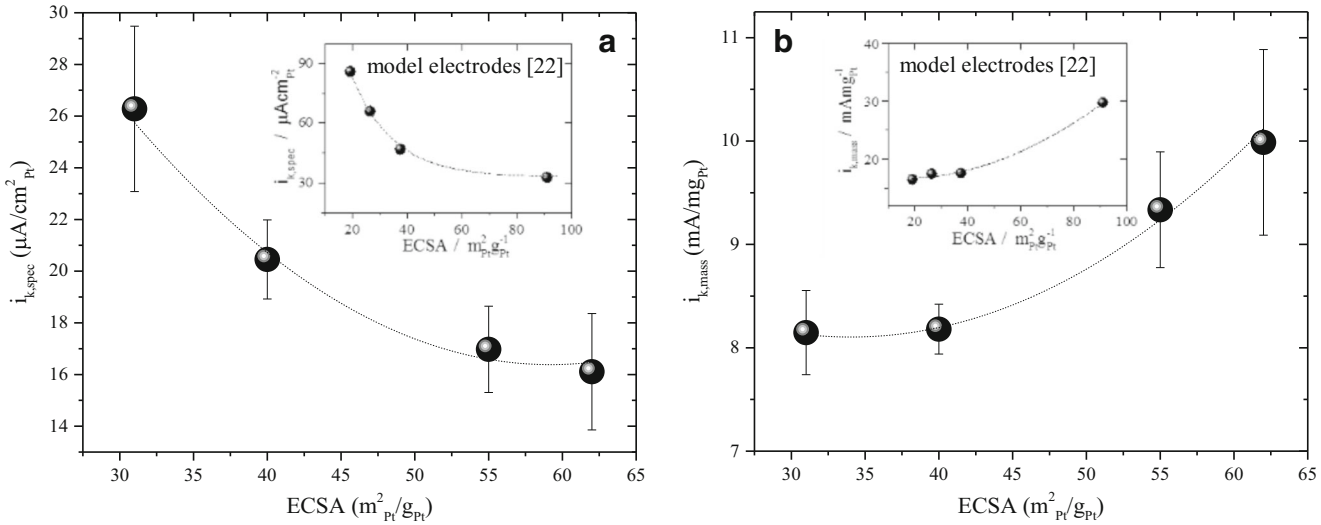

Fig. 6 Comparison of **a** surface-specific and **b** mass activity for the oxygen reduction reaction measured at 0.9 V vs. RHE for model electrodes [21] (*inserts*) and catalysts prepared in this work (*main curve*) versus wt% Pt

carbon, i.e. only the top surface of the carbon as defined by the geometric surface area and the roughness of the carbon layer exposed to the electrolyte have been (partially) covered. In the former, the Pt particles are spread over the whole surface of the carbon. Interparticle distance is known to have an effect on the formation of hydrogen peroxide species, which adversely affect ORR activity [4, 5, 15].

As previously reported by other members of our group, mass and specific activity trends of Pt catalysts can be fitted on a so-called master curve [3, 21]. The master curve is obtained by normalising the values from different studies [14, 21, 30–36] to the activity values at a Pt-specific surface area (35 $m^2 g_{Pt}^{-1}$) from the same study. By doing so, one can compare results obtained with different experimental conditions and varying data workup. In Fig. 7, mass (Fig. 7a) and specific activities (Fig. 7b) from this and other studies are plotted on such a curve.

It can be seen that all results, including the ones obtained using our system, show an increase in mass activity and a decrease in specific activity with increasing ECSA. An increase in ECSA can be the result of either a decrease in particle size or a change from agglomerated Pt particles to isolated Pt nanoparticles as is the case here.

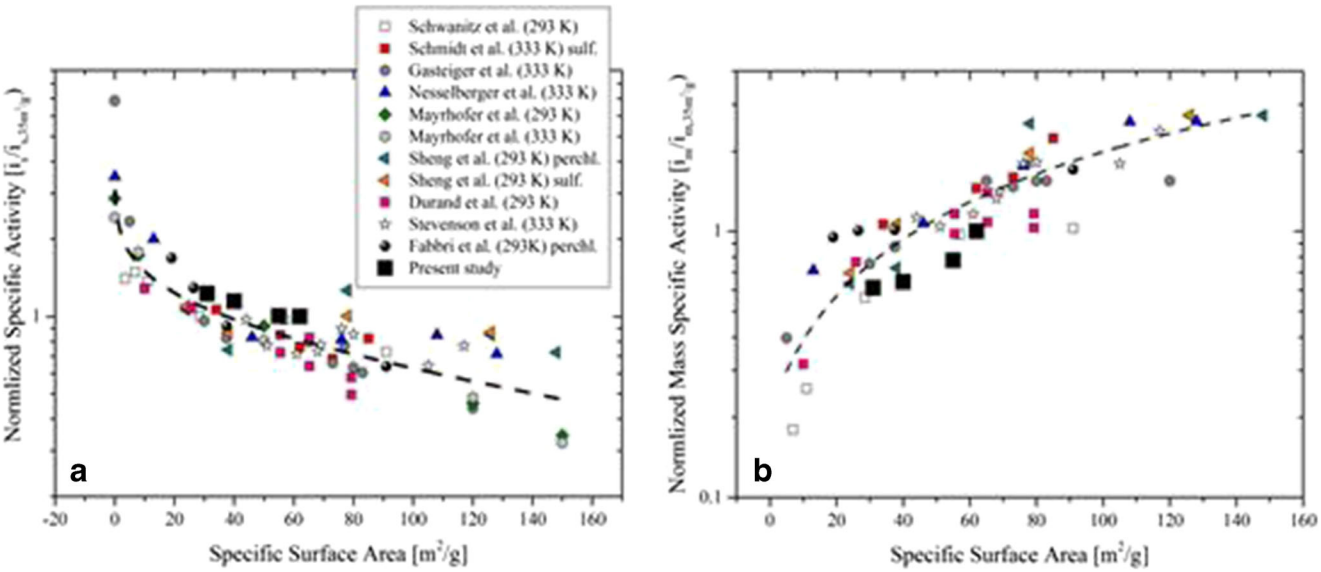

Fig. 7 **a** Mass and **b** specific activity towards the ORR at 0.9 V vs. RHE for different Pt catalysts normalised to the respective current values at 35 m^2/g_{Pt}. ORR activities are taken from measurements by Schwanitz et al. [14], Fabbri et al. [21], Schmidt et al. [30], Gasteiger et al. [31], Nesselberger et al. [32], Mayrhofer at al. [33], Sheng et al. [34], Antoine et al. [35] and Stevenson and Pattrick [36]

Hydrogen Peroxide Formation—RRDE Study

RRDE measurements were used to assess the extent of peroxide formation on the different platinum surfaces of the low and high platinum loading catalysts. The fraction of peroxide formed relative to the overall current was calculated according to the following equation [17].

$$x_{H_2O_2}[\%] = 100 \cdot \frac{2Ir/N}{Id + Ir/N} \quad (6)$$

Figure 8 represents a simplified reaction scheme for the ORR [2]. According to the mechanism below, k_1 is a 'direct' reaction pathway involving a four-electron transfer forming H_2O with no intermediates. However, k_2 describes the reaction pathway whereby O_2 is first transformed to H_2O_2 by a two-electron transfer and may be further reduced to H_2O via k_3; if these reactions occur consecutively, this is known as the 'series reaction pathway'. The H_2O_2 intermediate may also be desorbed or disproportionate chemically via k_4.

The extent of H_2O_2 formation was determined for Vulcan XC72R deposited on the surface of a ring disk electrode. The amount of carbon deposited on the surface was the same as the carbon present for the 20 wt% catalyst, i.e. the greatest exposure of the carbon surface compared with the 40, 60 and 80 wt% catalysts. Figure 9 below illustrates the extent of H_2O_2 formation on the different platinum surfaces.

It is first of all clear that the contribution of hydrogen peroxide formed on the Vulcan XC72R surface is negligible, and therefore should not be taken into account in the following discussion. Hydrogen peroxide was detected at potentials below 0.8 V and the yield of H_2O_2 increased with decreasing potential. This indicates that the two-electron pathway does in fact occur on the surface of Pt/C catalysts. This confirms the work of Katsounaros et al. [1] who reported very high H_2O_2 formation activities for Pt at potentials lower than 0.8 V vs. RHE. A significant increase in H_2O_2 formation was observed at potentials <0.2 V. This can partly be attributed to the blockage of surface active sites by adsorbed hydrogen atoms, preventing the dissociative adsorption of oxygen molecules [15]. However, a recent DFT study by Eslamibidgoli and Eikerling [37] showed that the energetics and hydrophobicity of the surface change in different potential ranges. It is also noted that H_2O_2 formation on Pt agglomerates or high loading

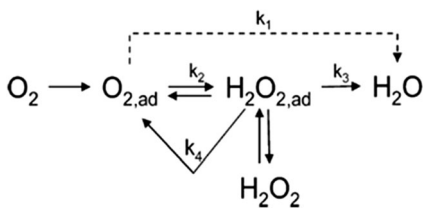

Fig. 8 Simplified reaction scheme for the oxygen reduction reaction *n*

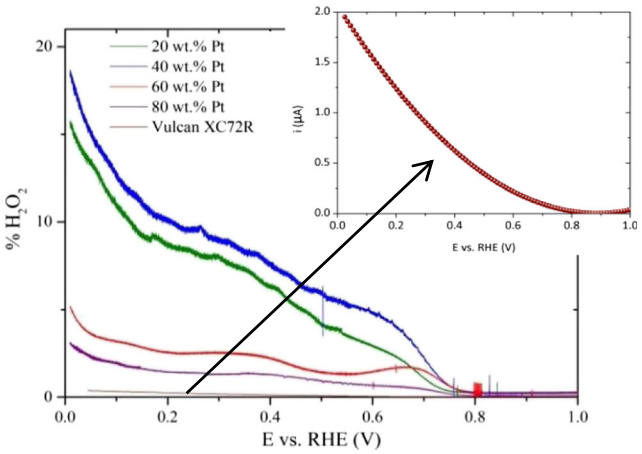

Fig. 9 H_2O_2 yield for oxygen reduction in an oxygen-saturated 0.1 M $HClO_4$ solution at room temperature. Rotation speed 1600 rpm H_2O_2 yield plotted versus disk potential

samples is the lowest. The higher specific activity observed for these samples could be related to the decreased H_2O_2 formation. The explanation for the lower H_2O_2 formation for the catalysts with the higher loadings can be found in the higher degree of agglomeration and smaller interparticle distances observed for these catalysts. There is a greater probability that a H_2O_2 species will be readsorbed on the same active site or a nearby active site for a Pt agglomerate than for an isolated Pt nanoparticle [2]. Therefore, the H_2O_2 can be further reduced to H_2O (via k_3, Fig. 7). This trend in H_2O_2 formation for the catalyst system prepared in this study agrees with the results of a recent investigation by our groups on a model system with increasing Pt loadings and suggests an ORR selectivity dependence on the Pt particle distribution [21].

Conclusions

In this work, we have shown the application of thermally induced chemical deposition to prepare a practical catalyst system with increasing Pt loadings. This resulted in the Pt surface morphology ranging from dispersed nanoparticles to agglomerates. We have investigated the correlation between the change in Pt surface morphology and ORR activity and selectivity. Furthermore, we have shown how H_2O_2 formation, desorption and readsorption is related to the Pt surface morphology and ORR activity. Using CO stripping voltammetry, the findings our groups previously reported, for a sputtered model system [21], could be confirmed in a practical catalyst system and the two systems show similar behaviour. A double voltammetric peak observed could be attributed to the presence of isolated platinum nanoparticles and platinum agglomerates. Finally, the detailed study of ORR activity and hydrogen peroxide formation showed that the formation of agglomerates at the higher Pt loadings causes the mass activity

of those catalysts to be significantly lower, as less active Pt surface is available for an electrochemical reaction. A drop in specific activity was also seen for lower Pt loadings. This observation could be related to the increased oxophilicity of Pt nanoparticles relative to Pt agglomerates. As such, lower specific activities are observed as a larger fraction of active Pt sites are essentially blocked by oxygen species; this was confirmed by our previous study and a similar trend of Pt-O peaks in the cyclic voltammograms for this study reveals the same conclusion. At lower Pt loadings (dispersed nanoparticles), too few active sites are available to readsorb the large quantities of H_2O_2 formed and react it further to form H_2O. This in turn suggests that the ORR largely proceeds via a sequential pathway via H_2O_2 species, rather than via direct reduction of O_2. This study could serve as a compass for further investigations into the particle size effects and the advantages of the electrocatalytic properties of extended platinum surfaces.

Acknowledgments ST, PL and OC thank the South African Department of Science and Technology for financial support in the form of HySA/Catalysis Centre of Competence programme funding (OC, PL) and a HySA/Catalysis student bursary (ST). ST further thanks PSI for research visit funding. The authors also acknowledge the Electron Microscopy Unit at the University of Cape Town for assistance with TEM imaging and the HR-TEM facilities at the University of the Western Cape (UWC, Cape Town, South Africa) for recording the STEM images.

References

1. I. Katsounaros, W.B. Schneider, J.C. Meier, U. Benedikt, P.U. Biedermann, A. Auer, K.J.J. Mayrhofer, Phys. Chem. Chem. Phys. **14**, 7384 (2012)
2. N.M. Markovic, T.J. Schmidt, V. Stamenkovic, P.N. Ross, Fuel Cells **1**, 105 (2001)
3. A. Rabis, P. Rodriguez, T.J. Schmidt, ACS Catal. **2**, 110 (2012)
4. H. Yang, S. Kumar, S. Zou, J. Electroanal. Chem. **688**, 180 (2013)
5. M. Nesselberger, M. Roezfaad, R. Fayçal Hamou, P.U. Biedermann, F. Schweinberger, S. Kunz, K. Schloegl, G. Wiberg, S. Ashton, U. Heiz, K.J.J. Mayrhofer, M. Arenz, Nat. Mater. **12**, 1 (2013)
6. M.K. Debe, Nat. Mater. **486**, 43 (2012)
7. V. Stamenkovic, B. Fowler, B.S. Mun, G. Wang, P.N. Ross, C.A. Lucas, N.M. Markovic, Science **315**, 493 (2012)
8. K.J.J. Mayrhofer, D. Strmcnik, B.B. Blizanac, V. Stamenkovic, M. Arenz, N.M. Markovic, Electrochim. Acta **53**, 3181 (2008)
9. Z. Xu, H. Zhang, H. Zhong, Q. Lu, Y. Wang, D. Su, Appl. Catal. B **111–112**, 264 (2012)
10. K. Kinoshita, J. Electrochem. Soc. **137**, 845 (1990)
11. W. Romanowski, Surf. Sci. **18**, 373 (1969)
12. R. Van Hardeveld, F. Hartog, Surf. Sci. **15**, 189 (1969)
13. M. Shao, A. Peles, K. Shoemaker, Nano Lett. **11**, 3714 (2011)
14. B. Schwanitz, A. Rabis, M. Horisberger, G.G. Scherer, T.J. Schmidt, Chimia **66**, 110 (2012)
15. M. Inaba, H. Yamada, J. Tokunaga, A. Tasaka, Electrochem. Solid-State Lett. **7**, A474 (2004)
16. I. Katsounaros, J.C. Meier, K.J.J. Mayrhofer, Electrochim. Acta **110**, 790 (2013)
17. F. Maillard, S. Schreier, M. Hanzlik, E.R. Savinova, S. Weinkauf, U. Stimming, Phys. Chem. Chem. Phys. **7**, 385 (2005)
18. E.G. Ciapina, S.F. Santos, E.R. Gonzalez, J. Electroanal. Chem. **644**, 132 (2010)
19. A. López-Cudero, A. Cuesta, C. Gutiérrez, J. Electroanal. Chem. **579**, 1 (2005)
20. P. Urchaga, C. Coutanceau, G. Jerkiewicz, Langmuir **28**, 3658 (2012)
21. E. Fabbri, S. Taylor, A. Rabis, P. Levecque, O. Conrad, R. Koetz, T.J. Schmidt, ChemCatChem **6**, 1410 (2014)
22. T.J. Schmidt, H.A. Gasteiger, G.D. Stäb, P.M. Urban, D.M. Kolb, R.J. Behm, J. Electrochem. Soc. **145**, 2354 (1998)
23. Y. Garsany, I.L. Singer, K.E. Swider-Lyons, J. Electroanal. Chem. **662**, 396 (2011)
24. S. Trasatti, O.A. Petrii, Pure Appl. Chem. **63**, 711 (1991)
25. U.A. Paulus, T.J. Schmidt, H.A. Gasteiger, R.J. Behm, J. Electroanal. Chem. **495**, 134 (2001)
26. O. Antoine, R. Durand, J. Appl. Electrochem. **30**, 839 (2000)
27. A. López-Cudero, J. Solla-Gullón, E. Herrero, A. Aldaz, J.M. Feliu, J. Electroanal. Chem. **644**, 117 (2010)
28. B.C. Han, C.R. Miranda, G. Ceder, Phys. Rev. B **77**, 075410 (2008)
29. W. Chrzanowski, A. Wieckowski, Langmuir **14**, 1967 (1998)
30. T.J. Schmidt, N.M. Markovic', P.N. Ross, unpublished results
31. H.A. Gasteiger, S.S. Kocha, B. Sompalli, F.T. Wagner, Appl. Catal. B Environ. **56**, 9 (2005)
32. M. Nesselberger, S. Ashton, J.C. Meier, I. Katsounaros, K.J.J. Mayrhofer, M. Arenz, J. Am. Chem. Soc. **133**, 17428 (2011)
33. K.J.J. Mayrhofer, B.B. Blizanac, M. Arenz, V.R. Stamenkovic, P.N. Ross, N.M. Markovic, J. Phys. Chem. B **109**, 14433 (2005)
34. W.C. Sheng, S. Chen, E. Vescovo, Y. Shao-Horn, J. Electrochem. Soc. **159**, B96 (2012)
35. O. Antoine, Y. Bultel, R. Durand, J. Electroanal. Chem. **499**, 85 (2001)
36. M. Stevenson, G. Pattrick, unpublished results
37. M.J. Eslamibidgoli, M.H. Eikerling, ACS Catal. **5**, 6090 (2015)
38. Q. Naidoo, S. Naidoo, L. Petrik, A. Nechaev, P. Ndungu, Int. J. Hydrog. Energy **37**, 9459 (2012)